energies

MDPI

Article

The Evaluation of the Corrosion Rates of Alloys Applied to the Heating Tower Heat Pump (HTHP) by Machine Learning

Qingqing Liu, Nianping Li *, Yongga A, Jiaojiao Duan and Wenyun Yan

College of Civil Engineering, Hunan University, Changsha 410081, China; qingqingliu@hnu.edu.cn (Q.L.); ayg5120@hnu.edu.cn (Y.A.); duanjj@hnu.edu.cn (J.D.); yanwenyun@hnu.edu.cn (W.Y.)
* Correspondence: linianping@hnu.edu.cn

Abstract: The corrosion rate is an important indicator describing the degree of metal corrosion, and quantitative analysis of the corrosion rate is of great significance. In the present work, the support vector machine (SVM) and the artificial neural network (ANN) integrating the k-fold split method and the root-mean-square prop (RMSProp) optimizer are used to evaluate the corrosion rates of alloys, i.e., copper H65, aluminum 3003, and 20# steel, applied to the heating tower heat pump (HTHP) in various anti-freezing solutions at different corrosion times, flow velocities, and temperatures. The mean-square error (MSE) versus the epoch of the ANN model shows that the result breaks the local minimum and is at or close to the global minimum. Comparisons of the SVM-/ANN-evaluated corrosion rates and the measured ones show good agreements, demonstrating the good reliability of the obtained SVM and ANN models. Moreover, the ANN model is recommended since it performs better than the SVM model according to the obtained R^2 value. The present work can be further applied to predicting the corrosion rate without any prior experiment for improving the service life of the HTHP.

Keywords: corrosion rate; alloys; heating tower heat pump (HTHP); support vector machine (SVM); artificial neural network (ANN); machine learning

check for updates

Citation: Liu, Q.; Li, N.; A, Y.; Duan, J.; Yan, W. The Evaluation of the Corrosion Rates of Alloys Applied to the Heating Tower Heat Pump (HTHP) by Machine Learning. *Energies* **2021**, *14*, 1972. https://doi.org/10.3390/en14071972

Academic Editor: Luca Pasquini

Received: 25 February 2021
Accepted: 31 March 2021
Published: 2 April 2021

Publisher's Note: MDPI stays neutral with regard to jurisdictional claims in published maps and institutional affiliations.

Copyright: © 2021 by the authors. Licensee MDPI, Basel, Switzerland. This article is an open access article distributed under the terms and conditions of the Creative Commons Attribution (CC BY) license (https://creativecommons.org/licenses/by/4.0/).

1. Introduction

According to the International Energy Agency (IEA), calculation results for the global energy consumption in the field of construction, the global construction industry (including house construction and infrastructure construction), and end-use energy related to building operation accounted for 35% of the global energy consumption in 2018. Among these, the end-use energy of building construction and infrastructure construction accounted for 6%, while the energy consumed by building operation accounted for 30% of the global energy consumption. Moreover, in the construction sector, heating and cooling consume more than 60% of the overall energy consumption [1]. Therefore, reducing air-conditioning energy consumption and developing renewable energy are critical ways to building a resource-saving and environment-friendly society.

The heating tower heat pump (HTHP) is a convenient heating and cooling source for air-conditioning. The detailed strategy of the HTHP system is illustrated in Figure 1. As shown in Figure 1, the cold anti-freezing solution is sprayed from the top of the tower during heating; this solution comes in contact with air and thus absorbs the sensible and latent heat energy from the air. Subsequently, the solution is sent into the evaporator, where the heat energy can be transferred from the solution to the refrigerant. Therefore, the anti-freezing solution is cold again and then is pumped back to the heating tower for the next circulation. In the heat pump system, the heat energy absorbed by the heating tower is transferred to the indoor environment through the reverse Carnot cycle. In summer, the system stores the anti-freezing solution in a liquid storage tank to avoid solution waste and environmental pollution. Meanwhile, the system injects water into circulation, and the heat source tower

functions as a cooling tower. Thus, there is no issue of frosting for the HTHP system during running [2–4].

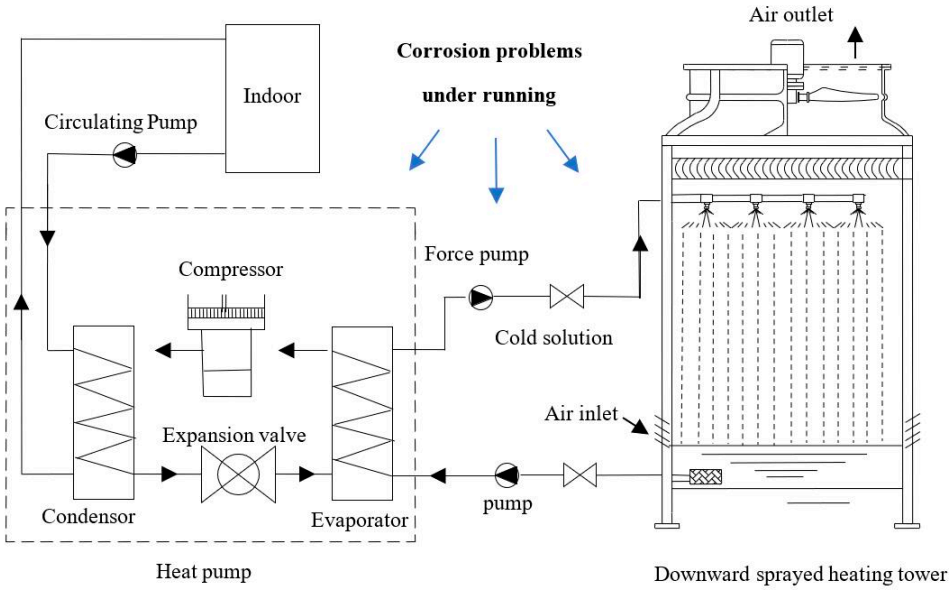

Figure 1. Schematic diagram of the heating tower heat pump (HTHP).

Therefore, the HTHP has unique advantages and has been widely researched and applied. However, the current research on HTHP mainly focuses on operating characteristics and structural optimization [5–7]. To summarize, Liang et al. [8] built an experimental platform for the HTHP to study the heat transfer performance of the open heating tower at different temperatures of the inlet solutions. Huang [9] studied the laws and design methods of heat and mass transfer, the characteristics and optimization of system operation, and the performance evaluations of the heating tower by combining theory, simulation, and experiment. Su [10] used a 25% NaCl solution as the anti-freezing solution to build a cross-flow HTHP system in Tianjin, China, to explore the feasibility of the HTHP system in winter, when the temperature and humidity are low. Lv [11] studied the optimization of the structure of the heating tower. However, in the HTHP system, the key equipment, such as heat exchangers and pipelines, is all metal and anti-freezing solutions (such as calcium chloride, ethylene glycol, lithium bromide, and other salt solutions) are corrosive to metals. The corrosion of the HTHP system can not only reduce the productivity during running but also increase the energy consumption and maintenance costs and even lead to the loss of commercial income during downtime. Figure 2 was shot for the HTHP system applied in one project in Changsha, China, in which Figure 2a presents the part inside the removed pipe from the HTHP system and Figure 2b shows the anti-freezing solution dissolving the corrosion product. From Figure 2, it can be clearly seen that the corrosion problems for the HTHP system are serious, which can lead to not only wastage of resources but also pollution of the environment. Thus, corrosion of the HTHP system should receive more attention from researchers [12,13]. Corrosion is commonly referred to as rust. BS EN ISO 8044 formally defines corrosion as "physicochemical interaction between a metal and its environment that leads to changes in properties of the metal and that may result in the significant impairment of the function of the metal, the environment, or the technical system, of which these form a part" [14]. Corrosion of metals and alloys is a critical issue in industry fields worldwide that is deleterious to both safety and environment and can also generate huge economic and energy costs [15,16]. Therefore, study of the methods to accurately measure and predict corrosion can contribute to saving both economic and energy costs.

(**a**) (**b**)

Figure 2. The corrosion problems occurring under the running of the HTHP for: (**a**) the pipes and (**b**) the anti-freezing solution.

The most commonly used method of measuring the corrosion rate is the corrosion coupon, which involves suspending a metal coupon with the same components as the ones for the practical application, such as pipes and heat exchangers, in a suitable solution. After some time, the metal coupon is taken out and the corresponding weight loss is measured, which can be then transformed into the corrosion rate using the following equations:

$$\text{Rate of weight loss}: \ V_{-} = \frac{W_1 - W_2}{A \cdot t} \tag{1}$$

$$\text{Rate of weight gain}: \ V_{+} = \frac{W_2 - W_1}{A \cdot t} \tag{2}$$

where $V_{\pm}$ (g/m^{2}h) represents the rate of weight loss/gain, W_1 (g) the initial mass of the metal, W_2 (g) the mass of the metal after corrosion treatment and drying, A (m^2) the surface area of the test piece, and t (h) the corrosion time of the coupon [17].

By using this method, Zhang [18] measured the corrosion rates of copper H65, aluminum 3003, and 20# steel in different anti-freezing solutions at various temperatures, corrosion times, and flow velocities. Zhang selected sodium acetate, magnesium chloride, and ethylene glycol as the primary materials and prepared six anti-freezing solutions of different compositions. Since the thermal conductivities of these prepared solutions are close to that of water and the thermophysical properties are generally good, these anti-freezing solutions are suitable for the HTHP system and should be further investigated. However, no quantitative analysis has been given in the available literature of the relationship between the corrosion rate and the various conditions. It is well known that the support vector machine (SVM) and the artificial neural network (ANN) are powerful mathematical methods to find the mapping relationship between input parameters and output parameters and have already been used in many fields, such as biology, medicine, and economy. [19–22]. Therefore, to perform quantitative analysis of the corrosion rate that can contribute to the prediction without any prior experiment, both SVM and ANN models are applied in the present work.

2. Models

2.1. Support Vector Machine

The support vector machine (SVM) is one of the common machine learning methods that can be applied to conduct classification and regression. In this work, for regression, the SVM is applied, which can map the input space to a high-dimension space by using a kernel function. In the high-dimension space, linear regression is then performed to obtain

the best model [23]. In the present work, the radial basis function (RBF) [24] is selected as the kernel function, which can be expressed as follows:

$$K(\mathbf{x}_i, \mathbf{x}_j) = \exp(-\frac{\|\mathbf{x}_i - \mathbf{x}_j\|^2}{2\sigma^2}) \quad (3)$$

The final model represented by the kernel function is

$$f(\mathbf{x}) = \sum_{i=1}^{N} (\alpha_i - \alpha_i^*) K(\mathbf{x}, \mathbf{x}_i) + b \quad (4)$$

where α_i and α_i^* are Lagrange multipliers and b the bias. After optimization using the experimental data, all the parameters can be obtained and the corresponding values can then be predicted by Equation (4) and the input x.

2.2. Artificial Neural Network

The artificial neural network includes three layers and several neurons in each layer. As shown in Figure 3, the first layer is the input layer, which contains the input features, i.e., the kind of metal material and anti-freezing solution, flow velocity, temperature, and corrosion time. The second layer is the hidden layer, which is used to connect the input layer and the output layer. The last one is the output layer, which represents the corrosion rate in the present work.

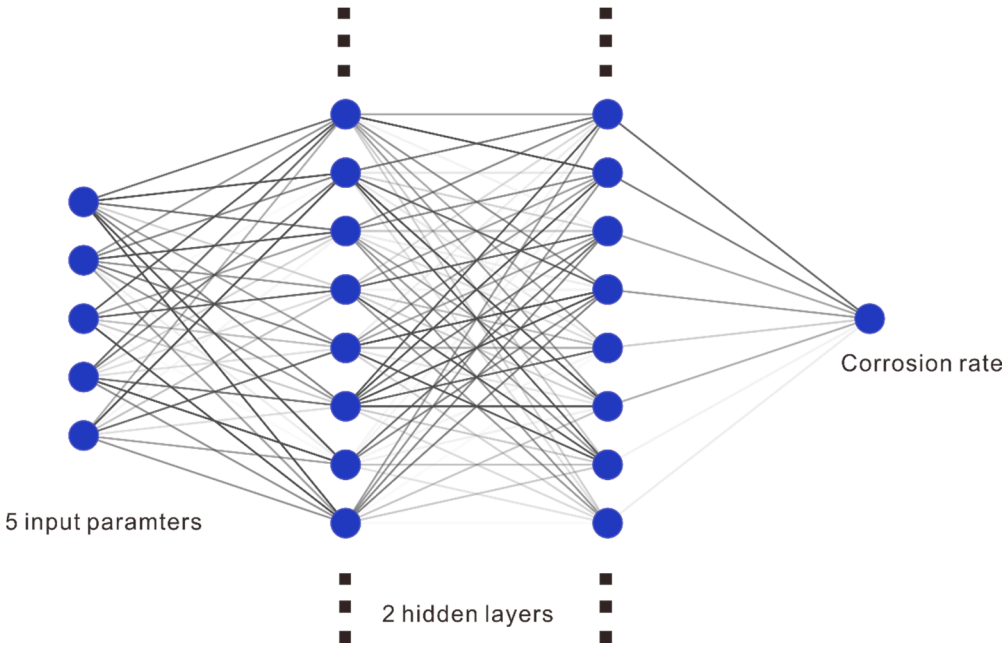

Figure 3. The structure of the artificial neural network (ANN) applied in the present work.

The number of hidden layers and the number of neurons in each hidden layer can critically affect the quality of the model, which can be adjusted according to the training performance. In each neuron, the linear superposition of all the connected neurons in the last layer and the activation function should be performed as shown in Figure 4, where w is the weight and b is the bias. It should be noted that the weights and bias in the linear superposition are what we should train and validate by the experimental data in order to find out the correct connection of the input and output layers. Meanwhile, in this work, the sigmoid function is chosen as the activation function since it can considerably improve

gradient exploding and gradient vanishing problems [25–27]. The sigmoid function is expressed as

$$f(x) = \frac{1}{1 + e^{-x}} \tag{5}$$

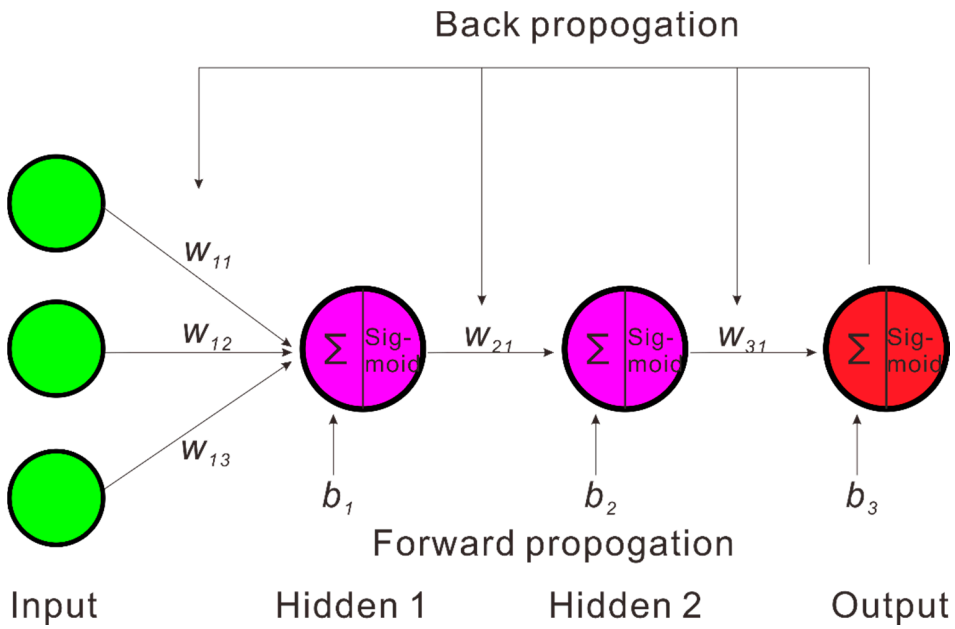

Figure 4. The strategy of forward propagation and back propagation.

The fully connected neural network used in this work is shown in Figure 4, where the neurons in green represent the three input features and the neuron in red represents the output corrosion rate. For the hidden layers, a two-layer structure is selected and each layer contains 10 neurons.

When training the neural network, the mean-square error (MSE) is selected as the metric of the loss function since this work is a kind of regression analysis. The purpose of training and validation is to minimize the MSE, which is shown as the following equation:

$$\text{MSE} = \frac{1}{n}\sum_{i=1}^{n}(Y_i - \hat{Y}_i) \tag{6}$$

where Y_i indicates the measured data and $\hat{Y}_i$ the predicted data. Meanwhile, the root-mean-square prop (RMSProp) is chosen as the optimizer, which can speed up the training rate [28,29]. To minimize the MSE, both forward propagation and back propagation should be performed. Forward propagation is to calculate the final output value through the network, which is shown in Figure 4. Back propagation is to adjust the weights and bias to minimize the MSE between evaluated output values and the measured ones by computing the gradient of the loss function with respect to each weight according to the chain rule.

3. Results and Discussion

As described in Section 2, the SVM and ANN were applied to evaluate the corrosion rates of copper H65, aluminum 3003, and 20# steel in different anti-freezing solutions at various corrosion times, temperatures, and flow velocities. It should be noted that copper H65, aluminum 3003, and 20# steel were, respectively, represented by 1, 2, and 3 in the SVM and ANN models, while the anti-freezing solutions BF2354, BK3000, BL3500, HG3500, YH6830, and ZP3682 were represented by 1–6, respectively, in the SVM and ANN models. Totally, five input parameters were considered in the present work, as shown in Figure 3.

The SVM-evaluated corrosion rate is shown in Figure 5 in comparison with the experimental ones, which shows an R^2 value of 0.9317. This result is reasonable but still not satisfactory. Meanwhile, to improve the reliability and accuracy of the ANN model, the k-fold cross validation was further used in the present work [30–34]. The main idea of k-fold cross validation is to choose different partitions of the training set and the validation set and then average the result so that the result will not be biased by any single partition. Moreover, k-fold cross validation is an effective way to solve the over-fitting problem. As shown in Figure 6, the dataset is first automatically split into k groups. Next, k-1 split groups are set to be the training dataset, and the one remaining split group is the validation dataset. Therefore, totally, k rounds of training and validation can be performed in one epoch, which critically improves the efficiency and accuracy. The value of k is often set to 5 or 10, depending on the computing resources. In the present work, k was set to 10 for achieving higher accuracy. Using the ANN model integrating the k-fold method, the MSE can be decreased much faster. The values of the MSE for the training dataset and the validation dataset along the epoch are shown in Figure 7. As can be seen in Figure 7, the MSE of the training dataset generally decreases with the increasing epoch and gets convergency. Meanwhile, the MSE of the validation dataset is critical to evaluating the predicting function of the obtained model. The MSE of the validation dataset first increases with the epoch and then decreases. After around 60,000 epoch, the MSE of the validation dataset cannot further decrease and becomes stable and convergent, demonstrating the best performance that can be achieved for the ANN model. Moreover, there is a local minimum for the validation MSE at about 5000 epoch. To break this local minimum, we used an optimizer called RMSProp, which can also adjust the training rate automatically to improve the efficiency. By using the RMSProp optimizer, this local minimum can be broken and thus the loss function can be close to the global minimum. We performed several tests for 100,000, 200,000, and 300,000 epoch, only to find that the MSE for the training dataset and the validation dataset can hardly decrease after about 60,000 epoch. Therefore, the minimum 100,000 epoch was chosen in the present work to show the result. The final MSE value for the training and validation datasets is 6.05×10^{-7} and 5.54×10^{-4}, respectively.

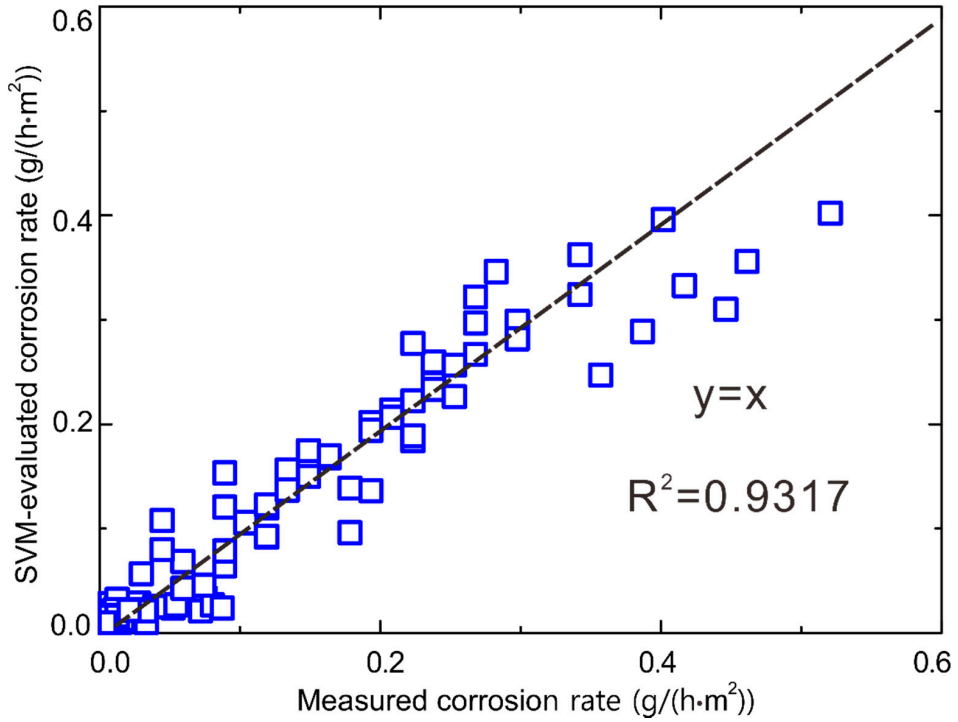

Figure 5. A comparison between support vector machine (SVM)-evaluated corrosion rates and measured ones.

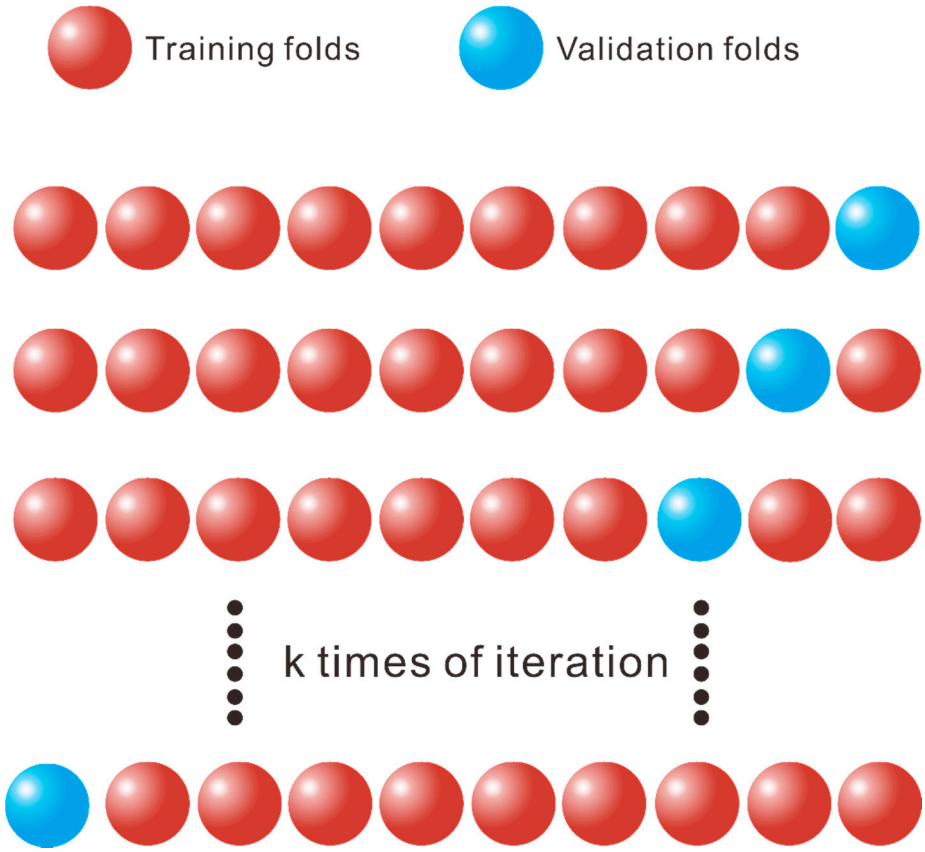

Figure 6. The strategy of k-fold split ones.

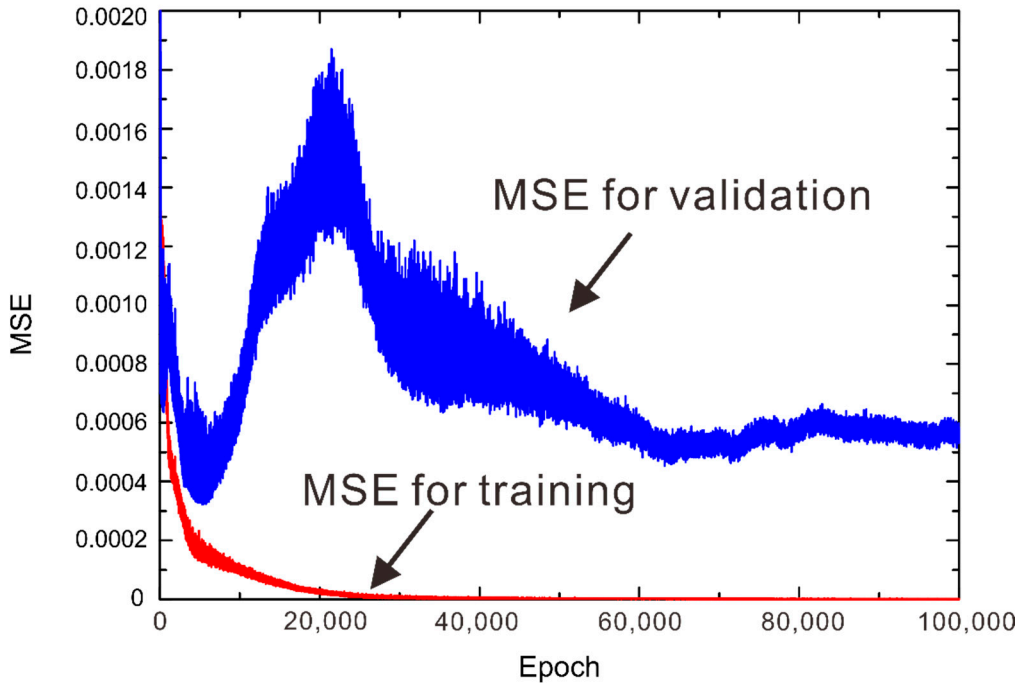

Figure 7. The mean-square error (MSE) of the ANN model along the epoch.

Subsequently, the ANN-evaluated corrosion rates were compared to the measured ones to further validate the reliability of the presently obtained ANN model. The comparison result is shown in Figure 8, where a good agreement can be seen since R^2 is 0.9974, demonstrating better reliability and accuracy of the ANN model than the SVM model. To

summarize, the SVM-/ANN-evaluated corrosion rates and the measured rates in different anti-freezing solutions at various temperatures, flow velocities, and corrosion times are all listed in Table 1.

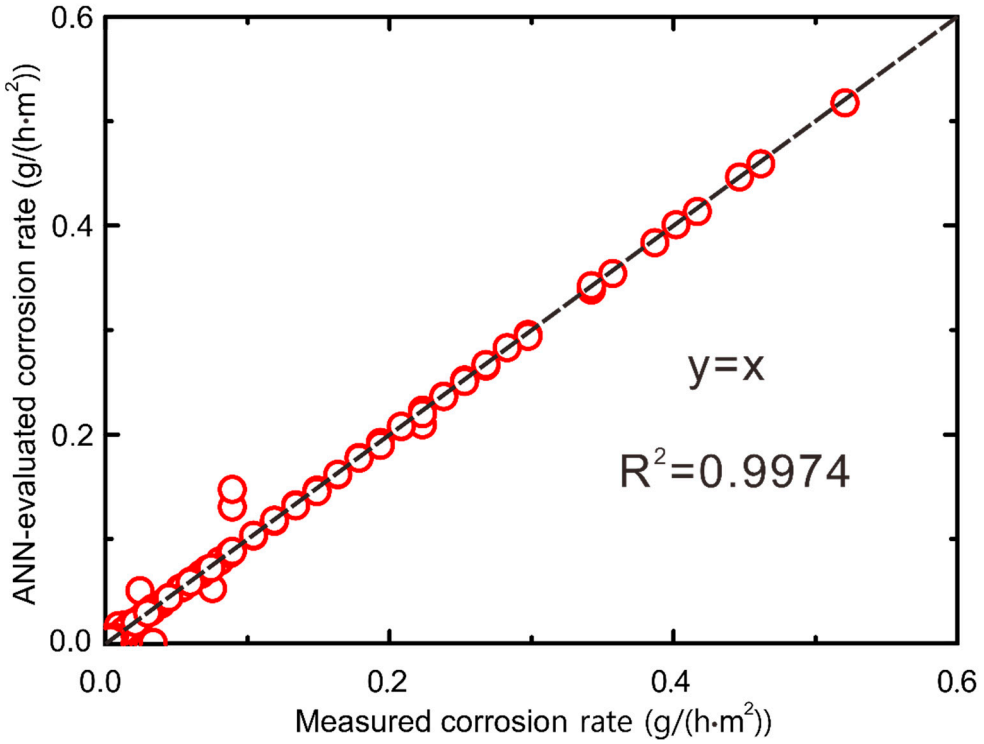

Figure 8. A comparison between ANN-evaluated corrosion rates and measured ones.

Table 1. Summary of the measured and ANN-evaluated corrosion rates of aluminum 3003, copper H65, and 20# steel in different anti-freezing solutions at different corrosion times, flow velocities, and temperatures.

Alloy	Coolant	Corrosion Time (Days)	Flow Velocity (m/s)	Temperature (°C)	Corrosion Rate (g/(h·m^2))			
					Measured	Uncertainty%	SVR-Evaluated	ANN-Evaluated
Copper H65	BF2354	30	0	15	0.07528	0.08	0.03276	0.05264
Aluminum 3003	BF2354	30	0	15	0.00805	0.74	0.01409	0.00796
20# Steel	BF2354	30	0	15	0.06005	0.10	0.03538	0.05975
Copper H65	HG3500	30	0	15	0.00259	2.31	0.01510	0.00260
Aluminum 3003	HG3500	30	0	15	0.00201	2.98	0.00443	0.00218
20# Steel	HG3500	30	0	15	0.01580	0.38	0.02249	0.01563
Copper H65	BK3000	30	0	15	0.00862	0.69	0.02358	0.00925
Aluminum 3003	BK3000	30	0	15	0.00575	1.04	0.00819	0.00550
20# Steel	BK3000	30	0	15	0.00201	2.98	0.02818	0.00222
Copper H65	BL3500	30	0	15	0.00517	1.16	0.01763	0.00548
Aluminum 3003	BL3500	30	0	15	0.00374	1.60	0.00494	0.00393
20# Steel	BL3500	30	0	15	0.05229	0.11	0.02384	0.05274
Copper H65	YH6830	30	0	15	0.00287	2.09	0.01605	0.00295
Aluminum 3003	YH6830	30	0	15	0.00575	1.04	0.00663	0.00580
20# Steel	YH6830	30	0	15	0.01207	0.50	0.02415	0.01209
Copper H65	ZP3682	30	0	15	0.01868	0.32	0.02035	0.01947
Aluminum 3003	ZP3682	30	0	15	0.01034	0.58	0.01143	0.01014
20# Steel	ZP3682	30	0	15	0.06723	0.09	0.02869	0.06643

Table 1. *Cont.*

Alloy	Coolant	Corrosion Time (Days)	Flow Velocity (m/s)	Temperature (°C)	Corrosion Rate (g/(h·m^2))			
					Measured	Uncertainty%	SVR-Evaluated	ANN-Evaluated
Copper H65	BF2354	30	0	10	0.02772	0.22	0.02878	0.02764
Aluminum 3003	BF2354	30	0	10	0.01076	0.56	0.01184	0.01052
20# Steel	BF2354	30	0	10	0.01265	0.47	0.03227	0.01239
Copper H65	HG3500	30	0	10	0.02045	0.29	0.01204	0.02026
Aluminum 3003	HG3500	30	0	10	0.00457	1.31	0.00294	0.00468
20# Steel	HG3500	30	0	10	0.02422	0.25	0.02024	0.05067
Copper H65	BK3000	30	0	10	0.01884	0.32	0.01989	0.01836
Aluminum 3003	BK3000	30	0	10	0.01319	0.45	0.00621	0.00446
20# Steel	BK3000	30	0	10	0.03929	0.15	0.02535	0.03791
Copper H65	BL3500	30	0	10	0.02018	0.30	0.01424	0.01953
Aluminum 3003	BL3500	30	0	10	0.00431	1.39	0.00321	0.00407
20# Steel	BL3500	30	0	10	0.07185	0.08	0.02130	0.07100
Copper H65	YH6830	30	0	10	0.00942	0.64	0.01330	0.00970
Aluminum 3003	YH6830	30	0	10	0.00807	0.74	0.00537	0.00810
20# Steel	YH6830	30	0	10	0.03337	0.18	0.02217	0.03379
Copper H65	ZP3682	30	0	10	0.03041	0.20	0.01791	0.03052
Aluminum 3003	ZP3682	30	0	10	0.00269	2.23	0.01036	0.00289
20# Steel	ZP3682	30	0	10	0.05463	0.11	0.02696	0.05413
Copper H65	BF2354	30	0	0	0.03144	0.19	0.02149	0.03034
Aluminum 3003	BF2354	30	0	0	0.00928	0.65	0.00846	0.00918
20# Steel	BF2354	30	0	0	0.08055	0.07	0.02680	0.07900
Copper H65	HG3500	30	0	0	0.00449	1.33	0.00662	0.00447
Aluminum 3003	HG3500	30	0	0	−0.00090	−6.65	0.00103	0.00012
20# Steel	HG3500	30	0	0	0.01737	0.34	0.01646	0.01738
Copper H65	BK3000	30	0	0	0.01228	0.49	0.01323	0.01748
Aluminum 3003	BK3000	30	0	0	0.00120	4.99	0.00336	0.00112
20# Steel	Bk3000	30	0	0	0.00449	1.33	0.02047	0.00426
Copper H65	BL3500	30	0	0	0.01228	0.49	0.00821	0.01194
Aluminum 3003	BL3500	30	0	0	0.00120	4.99	0.00086	0.00001
20# Steel	BL3500	30	0	0	0.00449	1.33	0.01699	0.00468
Copper H65	YH6830	30	0	0	0.01288	0.46	0.00845	0.01267
Aluminum 3003	YH6830	30	0	0	0.00299	2.00	0.00383	0.00292
20# Steel	YH6830	30	0	0	0.02126	0.28	0.01887	0.02090
Copper H65	ZP3682	30	0	0	0.02485	0.24	0.01359	0.02392
Aluminum 3003	ZP3682	30	0	0	0.00809	0.74	0.00912	0.00823
20# Steel	ZP3682	30	0	0	0.08744	0.07	0.02408	0.08610
Copper H65	BF2354	30	0	−10	0.01886	0.32	0.01547	0.01757
Aluminum 3003	BF2354	30	0	−10	0.03342	0.18	0.00680	0.00111
20# Steel	BF2354	30	0	−10	0.01125	0.53	0.02265	0.01039
Copper H65	HG3500	30	0	−10	0.00132	4.54	0.00245	0.00143
Aluminum 3003	HG3500	30	0	−10	0.00860	0.70	0.00070	0.00882
20# Steel	HG3500	30	0	−10	0.00794	0.75	0.01391	0.00815
Copper H65	BK3000	30	0	−10	0.00894	0.67	0.00787	0.00880
Aluminum 3003	BK3000	30	0	−10	0.00132	4.54	0.00222	0.00101
20# Steel	BK3000	30	0	−10	0.00199	3.01	0.01692	0.00194
Copper H65	BL3500	30	0	−10	0.00099	6.05	0.00348	0.00103
Aluminum 3003	BL3500	30	0	−10	0.00364	1.64	0.00017	0.00366
20# Steel	BL3500	30	0	−10	0.01655	0.36	0.01398	0.01623

Table 1. *Cont.*

Alloy	Coolant	Corrosion Time (Days)	Flow Velocity (m/s)	Temperature (°C)	Corrosion Rate (g/(h·m^2))			
					Measured	Uncertainty%	SVR-Evaluated	ANN-Evaluated
Copper H65	YH6830	30	0	−10	0.00364	1.64	0.00476	0.00349
Aluminum 3003	YH6830	30	0	−10	0.00496	1.21	0.00376	0.00760
20# Steel	YH6830	30	0	−10	0.01158	0.52	0.01669	0.00789
Copper H65	ZP3682	30	0	−10	0.01456	0.41	0.01028	0.01415
Aluminum 3003	ZP3682	30	0	−10	0.00993	0.60	0.00919	0.01119
20# Steel	ZP3682	30	0	−10	0.02118	0.28	0.02218	0.02088
Copper H65	BF2354	30	0	−15	0.00919	0.65	0.01306	0.01709
Aluminum 3003	BF2354	30	0	−15	0.00201	2.98	0.00668	0.00198
20# Steel	BF2354	30	0	−15	0.03274	0.18	0.02117	0.03165
Copper H65	HG3500	30	0	−15	−0.00057	−10.50	0.00094	0.00150
Aluminum 3003	HG3500	30	0	−15	0.00373	1.60	0.00119	0.00380
20# Steel	HG3500	30	0	−15	0.01551	0.39	0.01319	0.01517
Copper H65	BK3000	30	0	−15	0.00460	1.30	0.00581	0.00469
Aluminum 3003	BK3000	30	0	−15	0.00115	5.21	0.00236	0.00107
20# Steel	BK3000	30	0	−15	0.00287	2.09	0.01574	0.00275
Copper H65	BL3500	30	0	−15	0.00287	2.09	0.00172	0.00270
Aluminum 3003	BL3500	30	0	−15	0.00144	4.16	0.00052	0.00179
20# Steel	BL3500	30	0	−15	0.01666	0.36	0.01305	0.01696
Copper H65	YH6830	30	0	−15	0.00230	2.60	0.00345	0.00233
Aluminum 3003	YH6830	30	0	−15	0.00172	3.48	0.00433	0.00181
20# Steel	YH6830	30	0	−15	0.01264	0.47	0.01611	0.01202
Copper H65	ZP3682	30	0	−15	0.00632	0.95	0.00910	0.00619
Aluminum 3003	ZP3682	30	0	−15	0.00373	1.60	0.00978	0.00387
20# Steel	ZP3682	30	0	−15	0.02097	0.29	0.02167	0.02010
Copper H65	YH6830	1	0	15	0.17857	10.06	0.09596	0.17803
Copper H65	YH6830	1	0.5	15	0.19345	9.28	0.13628	0.19239
Copper H65	YH6830	1	1	15	0.22321	8.05	0.18418	0.20934
Copper H65	YH6830	1	1.5	15	0.23810	7.54	0.23871	0.23679
Copper H65	YH6830	1	2	15	0.29762	6.03	0.29862	0.29576
Copper H65	YH6830	1	2.5	15	0.34226	5.25	0.36238	0.33825
Copper H65	YH6830	1	0	0	0.05952	30.17	0.06847	0.05850
Copper H65	YH6830	1	0.5	0	0.10417	17.24	0.10518	0.10302
Copper H65	YH6830	1	1	0	0.14881	12.07	0.14989	0.14674
Copper H65	YH6830	1	1.5	0	0.19345	9.28	0.20174	0.19167
Copper H65	YH6830	1	2	0	0.23810	7.54	0.25952	0.23625
Copper H65	YH6830	1	2.5	0	0.26786	6.70	0.32177	0.26566
Copper H65	YH6830	1	0	−15	0.07440	24.14	0.04583	0.07231
Copper H65	YH6830	1	0.5	−15	0.08929	20.11	0.07862	0.13068
Copper H65	YH6830	1	1	−15	0.11905	15.09	0.11957	0.11780
Copper H65	YH6830	1	1.5	−15	0.16369	10.97	0.16789	0.16144
Copper H65	YH6830	1	2	−15	0.22321	8.05	0.22248	0.22012
Copper H65	YH6830	1	2.5	−15	0.29762	6.03	0.28192	0.29403
Aluminum 3003	BL3500	1	0	15	0.11905	15.09	0.09180	0.11736
Aluminum 3003	BL3500	1	0.5	15	0.17857	10.06	0.13890	0.17757
Aluminum 3003	BL3500	1	1	15	0.19345	9.28	0.19413	0.18953
Aluminum 3003	BL3500	1	1.5	15	0.25298	7.10	0.25640	0.25226
Aluminum 3003	BL3500	1	2	15	0.34226	5.25	0.32425	0.34253
Aluminum 3003	BL3500	1	2.5	15	0.40179	4.47	0.39597	0.40071

Table 1. *Cont.*

Alloy	Coolant	Corrosion Time (Days)	Flow Velocity (m/s)	Temperature (°C)	Corrosion Rate (g/(h·m^2))			
					Measured	Uncertainty%	SVR-Evaluated	ANN-Evaluated
Aluminum 3003	BL3500	1	0	0	0.08929	20.11	0.06441	0.08807
Aluminum 3003	BL3500	1	0.5	0	0.10417	17.24	0.10599	0.10350
Aluminum 3003	BL3500	1	1	0	0.13393	13.41	0.15609	0.13267
Aluminum 3003	BL3500	1	1.5	0	0.20833	8.62	0.21373	0.20775
Aluminum 3003	BL3500	1	2	0	0.22321	8.05	0.27758	0.22328
Aluminum 3003	BL3500	1	2.5	0	0.28274	6.35	0.34602	0.28306
Aluminum 3003	BL3500	1	0	−15	0.05952	30.17	0.04289	0.05865
Aluminum 3003	BL3500	1	0.5	−15	0.08929	20.11	0.07847	0.08803
Aluminum 3003	BL3500	1	1	−15	0.11905	15.09	0.12269	0.11693
Aluminum 3003	BL3500	1	1.5	−15	0.14881	12.07	0.17469	0.14543
Aluminum 3003	BL3500	1	2	−15	0.23810	7.54	0.23327	0.23658
Aluminum 3003	BL3500	1	2.5	−15	0.26786	6.70	0.29691	0.26711
20# Steel	HG3500	1	0	15	0.04464	40.23	0.10779	0.04397
20# Steel	HG3500	1	0.5	15	0.08929	20.11	0.15330	0.14748
20# Steel	HG3500	1	1	15	0.20833	8.62	0.20671	0.20808
20# Steel	HG3500	1	1.5	15	0.26786	6.70	0.26696	0.26697
20# Steel	HG3500	1	2	15	0.41667	4.31	0.33266	0.41335
20# Steel	HG3500	1	2.5	15	0.52083	3.45	0.40214	0.51756
20# Steel	HG3500	1	0	0	0.04464	40.23	0.07977	0.04391
20# Steel	HG3500	1	0.5	0	0.08929	20.11	0.12065	0.08815
20# Steel	HG3500	1	1	0	0.16369	10.97	0.16984	0.16211
20# Steel	HG3500	1	1.5	0	0.25298	7.10	0.22639	0.25071
20# Steel	HG3500	1	2	0	0.38690	4.64	0.28899	0.38353
20# Steel	HG3500	1	2.5	0	0.46131	3.89	0.35603	0.45923
20# Steel	HG3500	1	0	−15	0.02976	60.35	0.05674	0.02929
20# Steel	HG3500	1	0.5	−15	0.11905	15.09	0.09255	0.11791
20# Steel	HG3500	1	1	−15	0.13393	13.41	0.13682	0.13187
20# Steel	HG3500	1	1.5	−15	0.22321	8.05	0.18869	0.21997
20# Steel	HG3500	1	2	−15	0.35714	5.03	0.24697	0.35405
20# Steel	HG3500	1	2.5	−15	0.44643	4.02	0.31016	0.44662

The evaluation of the measurement uncertainty was further performed in the present work. The uncertainty of the electronic balance used in the present work is 0.1 mg, and thus the maximum uncertainty should be 0.2 mg because each metal sample is weighed twice, i.e., before and after corrosion. According to the calculation of the corrosion rate, the relative uncertainty can be finally obtained, which is also listed in Table 1. From Table 1, it can be concluded that parameters such as temperature and corrosion time can critically influence the accuracy of the measured results. The reason is that these parameters can influence the total weight variation of the metal samples before and after corrosion. If the total weight variation is much larger than the maximum uncertainty, i.e., 0.2 mg, the relative uncertainty caused by the electronic balance is less obvious, and vice versa. For example, as shown in Table 1, when the corrosion time is longer, the corrosion is more obvious and the relative error of the measurement result is smaller, which leads to higher accuracy.

4. Conclusions

The SVM and ANN models integrating the k-fold split method were used in the present work to evaluate the corrosion rates of copper H65, aluminum 3003, and 20# steel

in six anti-freezing solutions at different corrosion times, temperatures, and flow velocities. The conclusions are as follows:

- The SVM can be used to obtain a reasonable corrosion rate, the R^2 value being 0.9317.
- The MSE of the training dataset for the ANN decreases with the epoch and can be convergent. Meanwhile, there is a local minimum region broken by the presently used optimizer RMSProp for the MSE of the validation dataset. It can be concluded that after around 60,000 epoch, the obtained ANN model can achieve the best performance.
- The good agreement between the ANN-evaluated corrosion rate and the measured ones indicates that the presently obtained ANN model is of better accuracy and reliability since the R^2 value is 0.9974. The present work can contribute to the prediction of the corrosion rates of copper H65, aluminum 3003, and 20# steel without any prior experiments, thus improving the performance and service life of the HTHP.

Author Contributions: Conceptualization, Q.L. and N.L.; methodology, Q.L. and Y.A.; software, Q.L. and J.D.; validation, Q.L., J.D., and W.Y.; formal analysis, Q.L. and N.L.; investigation, Q.L. and W.Y.; resources, Q.L., N.L., and Y.A.; data curation, Q.L. and Y.A.; writing—original draft preparation, Q.L. and N.L.; writing—review and editing, J.D. and W.Y.; visualization, Y.A. and W.Y.; supervision, N.L.; project administration, N.L.; funding acquisition, N.L. All authors have read and agreed to the published version of the manuscript.

Funding: This research was funded by the Natural Science Foundation of China (grant number 51878255).

Institutional Review Board Statement: Not applicable.

Informed Consent Statement: Not applicable.

Data Availability Statement: All data and models used during the study appear in the submitted article.

Acknowledgments: The authors would like to acknowledge Dongyou Company for providing information about the application of the HTHP system.

Conflicts of Interest: The authors declare no conflict of interest.

References

1. Building Energy Research Center of Tsinghua University. *2020 Annual Report on China Building Energy Efficiency*; China Architecture & Building Press: Beijing, China, 2020; pp. 2–10.
2. Cui, H.; Li, N.; Wang, X.; Peng, J.; Li, Y.; Wu, Z. Optimization of reversibly used cooling tower with downward spraying. *Energy* **2017**, *127*, 30–43. [CrossRef]
3. Niksiar, A.; Rahimi, A. Energy and exergy analysis for cocurrent gas spray cooling systems based on the results of mathematical modeling and simulation. *Energy* **2009**, *34*, 14–21. [CrossRef]
4. Song, P.; Xiao, H.; Shi, W.; Li, X.; Wang, B.; Li, Z.; Zhang, Y.; Zhong, H. Experimental investigation on closed-type heating tower using glycerol solution. *Int. J. Refrig.* **2019**, *99*, 272–287. [CrossRef]
5. Cui, H.; Li, N.; Peng, J.; Cheng, J.; Li, S. Study on the dynamic and thermal performances of a reversibly used cooling tower with upward spraying. *Energy* **2016**, *96*, 268–277. [CrossRef]
6. Cui, H.; Li, N.; Peng, J.; Cheng, J.; Zhang, N.; Wu, Z. Modeling the particle scavenging and thermal efficiencies of a heat absorbing scrubber. *Build Environ.* **2017**, *111*, 218–227. [CrossRef]
7. Liu, J.; Sun, Y.; Wang, W.; Zhu, J. Performance evaluation of air source heat pump under unnecessary defrosting phenomena for nine typical cities in China. *Int. J. Refrig.* **2017**, *74*, 385–398. [CrossRef]
8. Liang, C.; Wen, X.; Liu, C.; Zhang, X. Performance analysis and experimental study of heat-source tower solution regeneration. *Energ Convers Manag.* **2014**, *85*, 596–602. [CrossRef]
9. Huang, S. Study on Optimization and Evaluation of Heating Tower Heat Pump System. Ph.D. Thesis, Southeast University, Nanjing, China, 2019.
10. Su, Z. Performance Analysis of Wet Heat Source Tower Heat Pump System under Winter Condition in North China. Master's Thesis, Tianjin University, Tianjin, China, 2010.
11. Lv, Z.; Liang, C.; Huang, S.; Zhang, X. Heat and mass transfer performance of porous corrugated packing in heat-source tower. *J. Cent. South Univ.* **2018**, *49*, 1003–1010.
12. Feng, Q.; Yan, B.; Chen, P.; Shirazi, S. Failure analysis and simulation model of pinhole corrosion of the refined oil pipeline. *Eng. Fail. Anal.* **2019**, *106*, 104177. [CrossRef]

13. Benea, L.; Simionescu, N.; Mardare, L. The effect of polymeric protective layers and the immersion time on the corrosion behavior of naval steel in natural seawater. *J. Mater. Res. Technol.* **2020**, *9*, 13174–13184. [CrossRef]
14. Faisal, D.; Ryan, W.; Vijay, S.; Mahroo, E.; Steve, M. Predicting Corrosion rate in Chilled HVAC Pipe Network: Coupon vs Linear Polarisation Resistance method. *Eng. Fail. Anal.* **2020**, *109*, 104261.
15. Ma, L.; Wang, J.; Zhang, D.; Huang, Y.; Huang, L.; Wang, P.; Qian, H.; Li, X.; Terryn, H.A.; Mole, J.M.C. Dual-action self-healing protective coatings with photothermal responsive corrosion inhibitor nanocontainers. *Chem. Eng. J.* **2021**, *404*, 127118. [CrossRef]
16. Tan, B.; Xiang, B.; Zhang, S.; Qiang, Y.; Xu, L.; Chen, S.; He, J. Papaya leaves extract as a novel eco-friendly corrosion inhibitor for cu in H_2SO_4 medium. *J Colloid Interf. Sci.* **2021**, *582*, 918–931. [CrossRef] [PubMed]
17. Duan, T.; Peng, W.; Ding, K.; Guo, W.; Hou, J.; Cheng, W.; Liu, S.; Xu, L. Long-term field exposure corrosion behavior investigation of 316L stainless steel in the deep sea environment. *Ocean Eng.* **2019**, *189*, 06405. [CrossRef]
18. Zhang, P. Experimental Research on Metal Corrosion Performance of Coolants on Cold and Heat Source Side in Heat Source Tower Heat Pump. Ph.D. Thesis, Hunan University, Changsha, China, 2019.
19. Kumari, S.; Tiyyagura, H.R.; Douglas, T.L.; Mohammed, E.A.; Adriaens, A.; Fuchs-Godec, R.; Mohan, M.K.; Skirtach, A.G. ANN prediction of corrosion behaviour of uncoated and biopolymers coated cp-Titanium substrates. *Mater Des.* **2018**, *157*, 35–51. [CrossRef]
20. Smuga-Kogut, M.; Kogut, T.; Markiewicz, R.; Słowik, A. Use of Machine Learning Methods for Predicting Amount of Bioethanol Obtained from Lignocellulosic Biomass with the Use of Ionic Liquids for Pretreatment. *Energies* **2021**, *14*, 243. [CrossRef]
21. Wu, J.; Zhang, G.; Zhang, Q.; Zhou, J.; Wang, Y. Artificial neural network analysis of the performance characteristics of a reversibly used cooling tower under cross flow conditions for heat pump heating system in winter. *Energ. Build.* **2011**, *43*, 1685–1693. [CrossRef]
22. Alimoradi, H.; Soltani, M.; Shahali, P.; Moradi Kashkooli, F.; Larizadeh, R.; Raahemifar, K.; Adibi, M.; Ghasemi, B. Experimental Investigation on Improvement of Wet Cooling Tower Efficiency with Diverse Packing Compaction Using ANN-PSO Algorithm. *Energies* **2021**, *14*, 167. [CrossRef]
23. Awad, M.; Khanna, R. *Efficient Learning Machines*; Apress: New York, NY, USA, 2015.
24. Quinonero-Candela, J.Q.; Rasmussen, C.E. A unifying view of sparse approximate Gaussian process regression. *J. Mach. Learn. Res.* **2005**, *6*, 1939–1959.
25. Yin, C.; Goudriaan, J.; Lantinga, E.A.; Vos, J.; Spiertz, H.J. A Flexible Sigmoid Function of Determinate Growth. *Ann. Bot* **2003**, *91*, 361–371. [CrossRef]
26. Wanto, A.; Windarto, A.P.; Hartama, D.; Parlina, I. Use of Binary Sigmoid Function And Linear Identity In Artificial Neural Networks For Forecasting Population Density. *J. Inf. Technol.* **2017**, *1*, 43–54. [CrossRef]
27. Han, J.; Moraga, C. The Influence of the Sigmoid Function Parameters on the Speed of Backpropagation Learning. *Lect. Notes Comput. Sci.* **1995**, *930*, 195–201.
28. Zou, F.; Shen, L.; Jie, Z.; Zhang, W.; Liu, W. A Sufficient Condition for Convergences of Adam and RMSProp. In Proceedings of the IEEE/CVF Conference on Computer Vision and Pattern Recognition (CVPR), Long Beach, CA, USA, 16–20 June 2019; pp. 11127–11135.
29. Tieleman, T.; Hinton, G. *RMSProp, COURSERA: Lecture 6.5-Neural Networks for Machine Learning*. 2012. Available online: https://www.coursera.org/.
30. Wiens, T.S.; Dale, B.C.; Boyce, M.S.; Kershaw, G.P. Three way k-fold cross-validation of resource selection functions. *Ecol. Model* **2008**, *212*, 244–255. [CrossRef]
31. Bengio, Y.; Grandvalet, Y. No unbiased estimator of the variance of k-fold cross-validation. *J. Mach. Learn. Res.* **2004**, *5*, 1089–1105.
32. Rodriguez, J.D.; Perez, A.; Lozano, J.A. Sensitivity analysis of k-fold cross validation in prediction error estimation. *IEEE Trans. Pattern Anal. Mach. Intell.* **2009**, *32*, 569–575. [CrossRef]
33. Fushiki, T. Estimation of prediction error by using K-fold cross-validation. *Stat. Comput.* **2011**, *21*, 137–146. [CrossRef]
34. Wong, T.T. Performance evaluation of classification algorithms by k-fold and leave-one-out cross vali-dation. *Pattern Recogn.* **2015**, *48*, 2839–2846. [CrossRef]